Interaction of spherical nanoparticles with a highly focused beam of light

Kürşat Şendur[1], William Challener[2], and Oleg Mryasov[2]

[1] *Sabanci University, Istanbul, 34956, Turkey*
[2] *Seagate Technology Research Center, Pittsburgh, PA 15222-4215, USA*

sendur@sabanciuniv.edu

Abstract: The interaction of a highly focused beam of light with spherical nanoparticles is investigated for linear and radial polarizations. An analytical solution is obtained to calculate this interaction. The Richards-Wolf theory is used to express the incident electric field near the focus of an aplanatic lens. The incident beam is expressed as an integral where the integrand is separated into transverse-electric (TE) and transverse-magnetic (TM) waves. The interaction of each TE and TM wave with a spherical nanoparticle is calculated using the Mie theory. The resulting analytical solution is then obtained by integrating the scattered waves over the entire angular spectrum. A finite element method solution is also obtained for comparison.

© 2008 Optical Society of America

References and links

1. A. Ashkin, "Acceleration and trapping of particles by radiation pressure," Phys. Rev. Lett. **24,** 156–159 (1970).
2. C. Godefroy and M. Adjouadi, "Particle sizing in a flow environment using light scattering patterns," Part. Part. Syst. Charact. **17,** 47–55 (2000).
3. A. C. Eckbreth, "Effects of laser-modulated particulate incandescence on Raman scattering diagnostics," J. Appl. Phys. **48,** 4473–4479 (1977).
4. N. Morita, T. Tanaka, T. Yamasaki, and Y. Yakanishi, "Scattering of a beam by a spherical object," IEEE Trans. Antennas Propag. **16,** 724–727 (1968).
5. W.-C. Tsai and R. J. Pogorzelski, "Eigenfunction solution of the scattering of beam radiation fields by spherical objects," J. Opt. Soc. Am. A **65,** 1457–1463 (1975).
6. W. G. Tam and R. Corriveau, "Scattering of electromagnetic beams by spherical objects," J. Opt. Soc. Am. **68,** 763–767 (1978).
7. J. S. Kim and S. S. Lee, "Scattering of laser beams and the optical potential well for a homogeneous sphere," J. Opt. Soc. Am. **73,** 303–312 (1983).
8. J. P. Barton, D. R. Alexander, and S. A. Schaub, "Internal and near-surface electromagnetic fields for a spherical particle irradiated by a focused laser beam," J. Appl. Phys. **64,** 1632–1639 (1988).
9. L. W. Davis, "Theory of electromagnetic beams," Phys. Rev. A **19,** 1177–1179 (1979).
10. J. P. Barton, D. R. Alexander, and S. A. Schaub, "Internal fields of a spherical particle illuminated by a tightly focused laser beam: Focal point positioning effects at resonance," J. Appl. Phys. **65,** 2900–2906 (1989).
11. J. P. Barton and D. R. Alexander, "Fifth-order corrected electromagnetic field components for a fundemental Gaussian beam," J. Appl. Phys. **66,** 2800–2802 (1989).
12. J. P. Barton, D. R. Alexander, and S. A. Schaub, "Theoretical determination of net radiation force and torque for a spherical particle illuminated by a focused laser beam," J. Appl. Phys. **66,** 4594–4602 (1989).
13. J. P. Barton, "Electromagnetic-field calculations for a sphere illuminated by a higher-order Gaussian beam. I. Internal and near-field effects," Appl. Opt. **36,** 1303–1311 (1997).
14. J. P. Barton, "Electromagnetic-field calculations for a sphere illuminated by a higher-order Gaussian beam. II. Far-field scattering," Appl. Opt. **37,** 3339–3344 (1998).
15. E. Wolf, "Electromagnetic diffraction in optical systems I. An integral representation of the image field," Proc. Roy. Soc. London Ser. A **253,** 349–357 (1959).

16. B. Richards and E. Wolf, "Electromagnetic diffraction in optical systems II. Structure of the image field in an aplanatic system," Proc. Roy. Soc. London Ser. A **253,** 358–379 (1959).
17. A. Hartschuh, E. J. Sánchez, X. S. Xie, and L. Novotny, "High-resolution near-field Raman microscopy of single-walled carbon nanotubes," Phys. Rev. Lett. **90,** 095503 (2003).
18. W. A. Challener, I. K. Sendur, and C. Peng, "Scattered field formulation of finite difference time domain for a focused light beam in dense media with lossy materials," Opt. Express **11,** 3160–3170 (2003).
19. K. Sendur, W. Challener, and C. Peng, "Ridge waveguide as a near field aperture for high density data storage," J. Appl. Phys. **96,** 2743–2752 (2004).
20. G. Mie, "Beiträge zur optik truber medien, speziell kolloida ler metallösungen" Ann. d. Physik **25,** 377– (1908).
21. M. Born and E. Wolf, *Principles of Optics* 5th ed. (Pergamon Press, Oxford, 1975), section 13.5.
22. J. M. Jin, *The Finite Element Method in Electomagnetics* (John Wiley & Sons, New York, NY, 2000).
23. E. D. Palik, *Handbook of Optical Constants of Solids* (Academic Press, San Diego, CA, 1998).

1. Introduction

The interaction of focused light with spherical particles has been of interest for various applications, such as optical levitation [1], particle sizing [2], and Raman scattering diagnostics [3]. Since optical tweezers allow manipulation of small spherical particles without any mechanical contact, the calculation and measurement of optical trapping forces have been of special interest. Strong trends toward nanoscience and nanotechnology make it necessary to achieve easy and cost-effective fabrication and manipulation of nanostructures. Therefore, the extension of the aforementioned applications to nanoscale particles is of great interest. These tools can help achieve easy assembly of nano-particle arrays, which has a number of potential applications ranging from optical communication systems to data storage. This requires a thorough understanding of the interaction of focused light with nanoparticles of various materials and shapes. At visible and infrared frequencies, the underlying physics of the interaction of focused light and nano-particles is complicated due to the behavior of metals as strongly coupled plasmas.

Although there has been much effort to understand the effect of various parameters related to the surface plasmon resonances on nanoparticles, the modeling studies in the literature do not include detailed descriptions of a focused beam of light. A plane wave is usually used to represent the incident beam of light to understand this interacton. Although, proper models of a highly focused beam of light have largely been omitted in the context of surface plasmons, there is considerable literature for the interaction of Gaussian beams with large dielectric spheres that does not support surface plasmon resonances. The interaction of Gaussian beams and homogeneous spheres has been studied [4, 5, 6, 7]. These studies mainly concentrate on the far field scattering from the spheres. Barton et al. [8] calculated internal and near-field electric field distributions by using a first-order focused fundamental Gaussian model of a laser beam developed by Davis [9]. Barton et al. investigated the dependence of structural resonance behavior on focal point positioning [10]. Barton and Alexander [11] obtained a mathematical expression for a fifth-order corrected Gaussian beam. Using these models, Barton et al. [12] calculated the net radiation force and torque for a spherical particle illuminated by a focused laser beam. Barton [13, 14] investigated the interaction between laser beams with various polarizations (radial, angular, arched, and helix) and spherical particles. Higher order Hermite-Gaussian modes were used to represent these polarizations, and scattering from spheres were investigated in the near-field [13] and far-field [14]. If the beams become more tightly focused, the aforementioned Gaussian beam representations become inaccurate for modeling a highly focused beam of light. Although a Gaussian beam is a more accurate representation of a highly focused beam compared to a plane wave representation, a Gaussian beam is still an inadequate model of a highly focused beam.

The Richards-Wolf theory [15, 16] provides an accurate representation for the incident beam near the focus of an aplanatic lens. A solution for the interaction of spherical particles with incident beams described by Richards-Wolf theory is necessary for applications that utilize a

highly focused beam of light. This is particularly crucial for applications that utilize metallic spheres supporting surface plasmons, since the interaction of different spectral components of the incident beam with metal plasma varies significantly.

This study addresses the interaction of spherical nanoparticles with highly focused incident beams defined by Richards-Wolf theory [15, 16]. Both metallic and dielectric nanoparticles are investigated. Another important contribution of this paper is the utilization of both linear and radial polarizations. Analytical studies in the literature have mostly concentrated on linearly polarized light. However, more sophisticated polarizations such as radially polarized focused beams have been used extensively to excite surface plasmons in experimental studies. There has been increasing interest in radially polarized focused light due to its favorable configuration to excite surface plasmons on cylindrical particles [17]. The analytical models in this study can be used to validate complicated 3-D modeling tools, such as finite-difference time domain (FDTD) [18] and finite element method (FEM) [19], which can later be used to model more complicated nanostructures. We also compare the results of a 3-D FEM model with the analytical model presented in this study.

This paper is organized as follows: In Sect. 2 we present the formulations for the linearly and radially polarized electric fields. Different components of the electric field vector are identified and plotted for both linear and radial polarizations. In Sect. 3, the formulation for the interaction of focused light with spherical nanoparticles is presented. A verification of the implementation is presented in Sect. 4 by comparing the analytical and FEM solutions. The results for different spherical nanoparticles are presented and discussed in Sect. 4. Concluding remarks appear in Sect. 5.

2. Focused field formulation

Many applications, such as optical storage and optical levitation, use highly focused optical beams. An accurate prediction of three-dimensional distributions of various polarizations requires proper analysis of the vector nature of the incident electromagnetic fields. Richards and Wolf developed a method for calculating the electric field semi-analytically near the focus of an aplanatic lens [15, 16]. Using Richards-Wolf method, we can obtain both transverse and longitudinal components near the focus. As we describe below, Richards and Wolf method can be used to obtain the electric field components for different polarizations. In this study, we utilize linear and radial polarizations. A highly focused beam with a linear polarization has a stronger transverse component than a longitudinal component. Radial polarization, on the other hand, has a stronger component in the longitudinal direction than the transverse direction. Due to this difference, linearly and radially polarized focused beams interact differently with the particles that are placed around the focal region.

The total electric field in the vicinity of the focus is given by

$$\mathbf{E}(\mathbf{r}_p) = -\frac{i}{\lambda} \int_0^\alpha d\theta \sin\theta \int_0^{2\pi} d\phi \, \mathbf{a}(\theta, \phi) \exp(-i\mathbf{k} \cdot \mathbf{r}_p) \tag{1}$$

where α is the half angle of the beam, $\mathbf{r}_p$ is the observation point

$$\mathbf{r}_p = x_p\hat{x} + y_p\hat{y} + z_p\hat{z} = r_p\cos\phi_p\hat{x} + r_p\sin\phi_p\hat{y} + z_p\hat{z} \tag{2}$$

and

$$\mathbf{k} = \frac{2\pi}{\lambda}(\sin\theta\cos\phi\hat{x} + \sin\theta\sin\phi\hat{y} - \cos\theta\hat{z}). \tag{3}$$

In Eqs. (2) and (3) λ is the wavelength in the medium, $r_p = \sqrt{x_p^2 + y_p^2}$, and $\phi_p = \arctan(y_p/x_p)$. In Eq. (1), $\mathbf{a}(\theta, \phi)$ is the weighting vector for a plane wave incident from the (θ, ϕ) direction.

Here it should be noted that $\mathbf{a}(\theta,\phi)$ is a polarization dependent quantity. $\mathbf{a}(\theta_i,\phi_j)$ is given as

$$\mathbf{a}(\theta,\phi) = \left[\begin{array}{c} \cos\theta\cos^2\phi + \sin^2\phi \\ \cos\theta\cos\phi\sin\phi - \cos\phi\sin\phi \\ \sin\theta\cos\phi \end{array} \right] \sqrt{\cos\theta}, \tag{4}$$

$$\mathbf{a}(\theta,\phi) = \left[\begin{array}{c} \cos\theta\cos\phi \\ \cos\theta\sin\phi \\ \sin\theta \end{array} \right] \sqrt{\cos\theta}, \tag{5}$$

for linear and radial polarizations, respectively. In Eqs. (4) and (5), the $\sqrt{\cos\theta}$ factor is applied to the incident beam for energy conservation in a solid immersion lens (SIL), but no other apodization is applied.

To obtain the electric field distributions for radial and linear polarizations, Eq. (1) can be evaluated using a numerical integration. Equation (1) is discretized as

$$\mathbf{E}(\mathbf{r}_p) = -\frac{i}{\lambda} \sum_{i=1}^{N_\theta+1} \sum_{j=1}^{N_\phi+1} \omega_{ij} \sin\theta_i \sqrt{\cos\theta_i} \mathbf{a}(\theta_i,\phi_j) \exp(-i\mathbf{k}_{ij}\cdot\mathbf{r}_p) \tag{6}$$
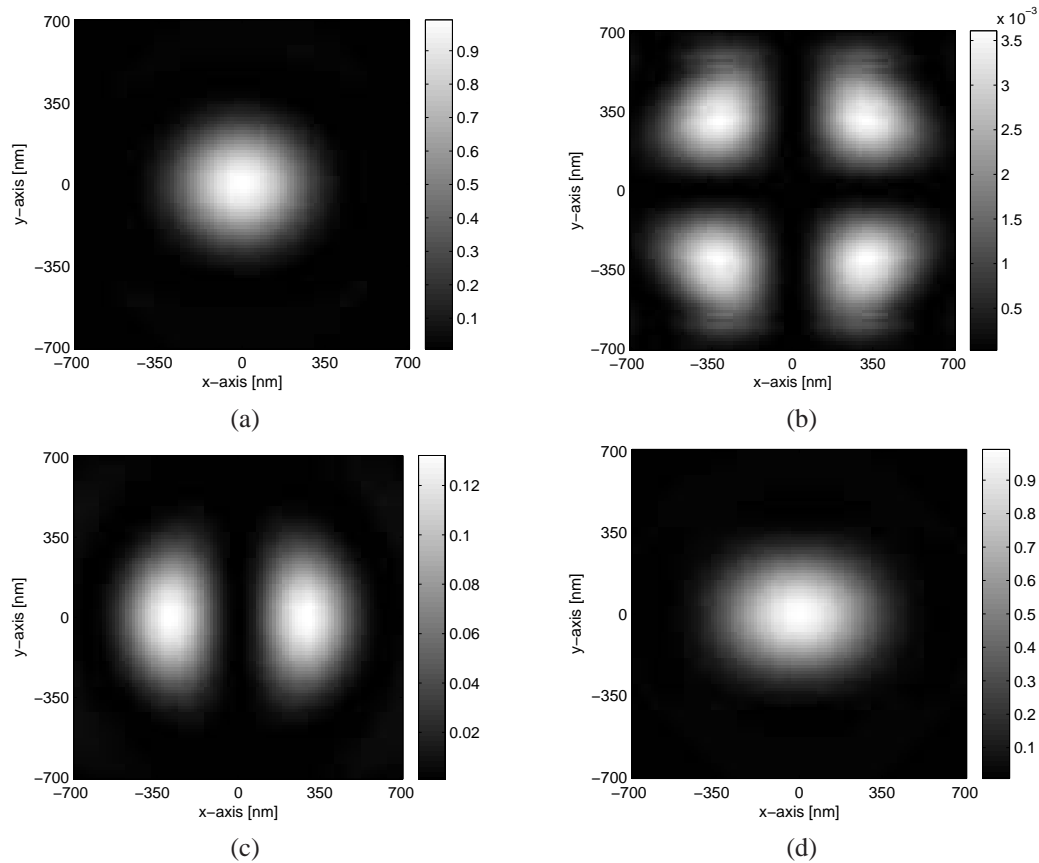
Fig. 1. Various electric fields components for the linearly polarized focused beam at the focal plane. The results are normalized with the maximum value of the total electric field. (a) $E_x(x,y)$, (b) $E_y(x,y)$, (c) $E_z(x,y)$, and (d) $E_t(x,y)$.

where ω_{ij} are the numerical quadrature coefficients,

$$\theta_i = \frac{(i-1)\theta_{max}}{N_\theta}, \tag{7}$$

$$\phi_j = \frac{(j-1)2\pi}{N_\phi}, \tag{8}$$

and

$$\mathbf{k}_{ij} = \frac{2\pi}{\lambda}(\sin\theta_i\cos\phi_j\hat{x} + \sin\theta_i\sin\phi_j\hat{y} - \cos\theta_i\hat{z}). \tag{9}$$

Using Eq. (6) along with Eqs. (4) and (5), we can now obtain the electric field distributions around the focus. Equation (6) can also be interpreted as a summation of plane waves propagating in the $\mathbf{k}_{ij}$ direction with an amplitude of $-\frac{i}{\lambda}\omega_{ij}\sin\theta_i\sqrt{\cos\theta_i}\mathbf{a}(\theta_i,\phi_j)$. Linear and radial polarizations are distinguished by the scaling factor $\mathbf{a}(\theta_i,\phi_j)$ of the plane wave in the $\mathbf{k}_{ij}$ direction.

Different components of the electric field are presented at the focal plane in Figs. 1 and 2 for linear and radial polarizations, respectively. In the calculations, the refractive index of the medium is 1, and the half angle of the beam is 60°. In both figures, the field quantities are

(a)

(b)

(c)

(d)
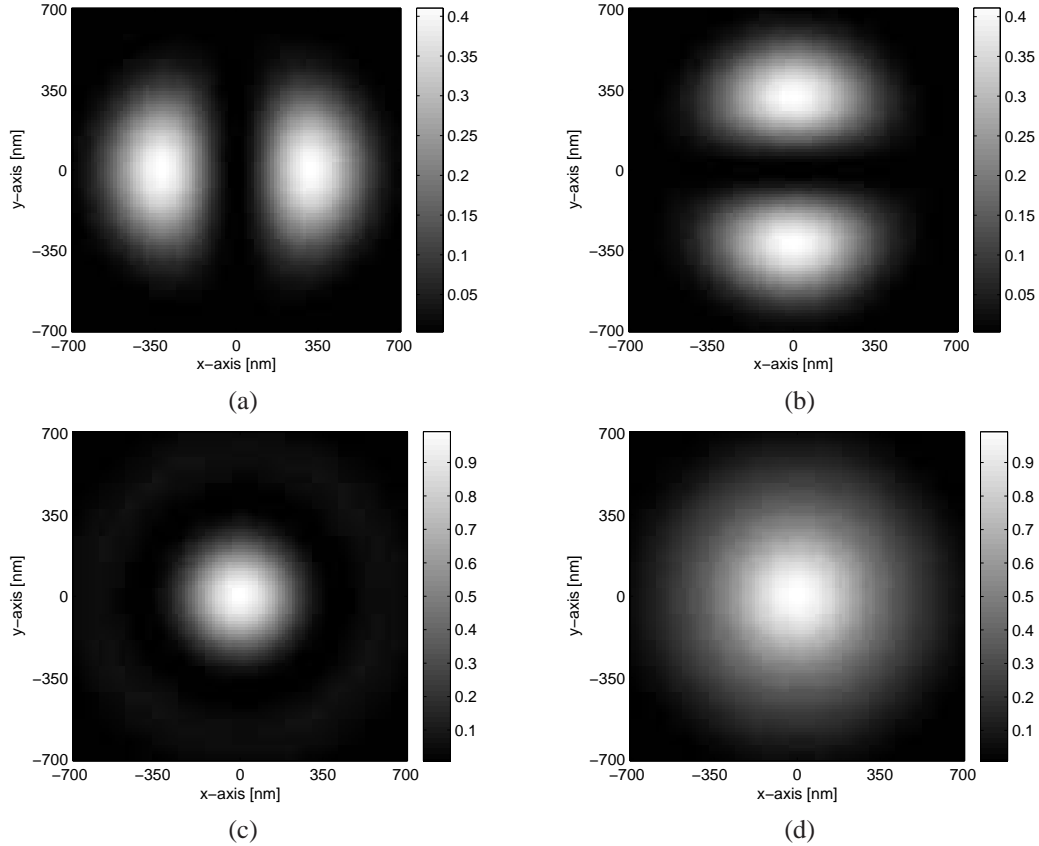
Fig. 2. Various electric fields components for the radially polarized focused beam at the focal plane. The results are normalized with the maximum value of the total electric field. (a) $E_x(x,y)$, (b) $E_y(x,y)$, (c) $E_z(x,y)$, and (d) $E_t(x,y)$.

normalized with the maximum value of the total electric field. For the linearly polarized focused wave, the x-component of the electric field is much stronger than the other two components as shown in Fig. 1. The radially polarized wave has a strong z-component in the focal region as shown in Fig. 2.

3. Analytical treatment of the interaction of focused light with spherical nanoparticles

In this section, the formulation for the interaction of focused light with spherical nanoparticles is presented. The incident focused light is described by Eq. (6) along with Eqs. (4) and (5) for linear and radial polarizations, respectively. In Eq. (6), a focused incident beam of light is expressed as an integral where the integrand can be separated into TE and TM polarized plane wave components. In our formulation, the interaction of each TE and TM plane wave component with a spherical nanoparticle is calculated using Mie theory. The resulting analytical solution is then obtained by integrating the scattered waves over the entire angular spectrum.

The technique summarized in this section is based on the Mie series solution for TE and TM plane waves. The interaction of plane waves with spheres has been thoroughly studied [20, 21] in the literature. In this study, we will not give explicit expressions for the Mie scattering problem, since it is well documented in the literature. However, we will utilize the results of Mie scattering problem to extend the formulations to scattering problems where the incident beam is defined by Richards-Wolf theory.

The most common solution for the Mie scattering solution has been given in the literature for a simple plane wave. A linearly polarized (in the x-direction) plane wave can be expressed as

$$\mathbf{E}_{inc}^{x}(\mathbf{r}) = \hat{x}\exp(i\mathbf{k}\cdot\mathbf{r}). \tag{10}$$

The presence of a spherical particle generates scattered fields. The solution of this problem is expressed as a total (incident + scattered) electric field $\mathbf{E}_{tot}^{x}(\mathbf{r})$. Explicit expressions for the $\mathbf{E}_{tot}^{x}(\mathbf{r})$ are given in the literature [21] as a summation of spherical harmonics, and will not be repeated here.

The TE$_{inc}$ and TM$_{inc}$ polarized incident plane waves, shown in Fig. 3, can be expressed as

$$\mathbf{E}_{inc}^{TE}(\mathbf{r}) = \left(-\sin\phi_{inc}\hat{x} + \cos\phi_{inc}\hat{y}\right)\exp(i\mathbf{k}\cdot\mathbf{r}), \tag{11}$$
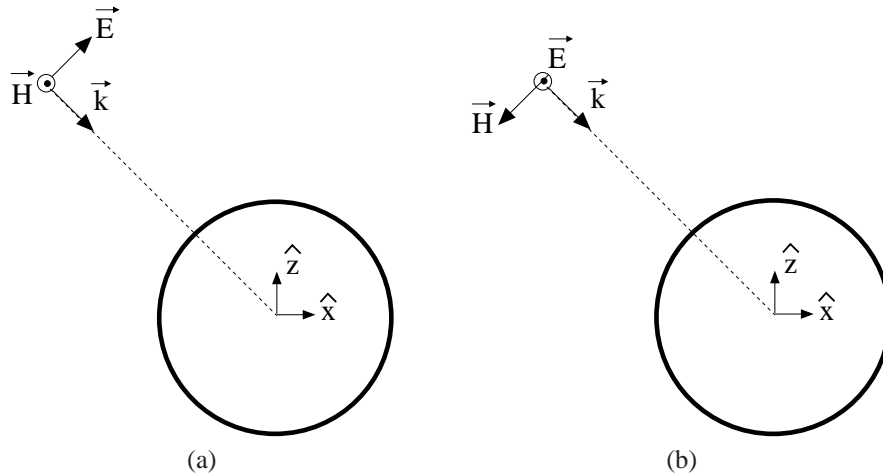
Fig. 3. Spherical particle illuminated by (a) TM polarized plane wave, and (a) TE polarized plane wave.

and

$$\mathbf{E}_{inc}^{TM}(\mathbf{r}) = \left(\cos\theta_{inc}\cos\phi_{inc}\hat{x} + \cos\theta_{inc}\sin\phi_{inc}\hat{y} + \sin\theta_{inc}\hat{z}\right)\exp(i\mathbf{k}\cdot\mathbf{r}), \qquad (12)$$

respectively. The incident $\mathbf{E}_{inc}^{TE}(\mathbf{r})$ and $\mathbf{E}_{inc}^{TM}(\mathbf{r})$ polarized plane waves in Eqs. (11) and (12) can be obtained from $\mathbf{E}_{inc}^{x}(\mathbf{r})$ in Eq. (10) by simple coordinate transformations. $\mathbf{E}_{inc}^{TM}(\mathbf{r})$ is obtained from $\mathbf{E}_{inc}^{x}(\mathbf{r})$ by subsequent $\theta = \theta_{inc}$, and $\phi = \phi_{inc}$ transformations. Similarly, $\mathbf{E}_{inc}^{TE}(\mathbf{r})$ is obtained from $\mathbf{E}_{inc}^{x}(\mathbf{r})$ by subsequent $\phi = -\pi/2$, $\theta = \theta_{inc}$, and $\phi = \phi_{inc}$ transformations. Since the incident fields $\mathbf{E}_{inc}^{TM}(\mathbf{r})$ and $\mathbf{E}_{inc}^{TE}(\mathbf{r})$ can be obtained from linear transformations of $\mathbf{E}_{inc}^{x}(\mathbf{r})$, the total fields $\mathbf{E}_{tot}^{TM}(\mathbf{r})$ and $\mathbf{E}_{tot}^{TE}(\mathbf{r})$ can be obtained from $\mathbf{E}_{tot}^{x}(\mathbf{r})$ by the same transformations due to the linearity of the system. In summary, the total electric fields due to the presence of the sphere $\mathbf{E}_{tot}^{TM}(\mathbf{r})$ and $\mathbf{E}_{tot}^{TE}(\mathbf{r})$ are obtained as

$$\mathbf{E}_{tot}^{TM}(\mathbf{r}) = \begin{bmatrix} \cos\theta\cos\phi & -\sin\phi & -\sin\theta\cos\phi \\ \cos\theta\sin\phi & \cos\phi & -\sin\theta\sin\phi \\ \sin\theta & 0 & \cos\theta \end{bmatrix} \mathbf{E}_{tot}^{x}(\mathbf{r}) \qquad (13)$$

$$\mathbf{E}_{tot}^{TE}(\mathbf{r}) = \begin{bmatrix} \sin\phi & \cos\theta\sin\phi & -\sin\theta\cos\phi \\ \cos\phi & \cos\theta\sin\phi & -\sin\theta\sin\phi \\ 0 & \sin\theta & \cos\theta \end{bmatrix} \mathbf{E}_{tot}^{x}(\mathbf{r}) \qquad (14)$$

So far, we have established how to obtain $\mathbf{E}_{tot}^{TM}(\mathbf{r})$ and $\mathbf{E}_{inc}^{TE}(\mathbf{r})$ starting from the expression in the literature. Equations (13) and (14) will be utilized to find the solution scattering from spherical particles when the incident field is given by Richards-Wolf theory. In Eq. (1), a highly focused incident beam of light is expressed as an integral where the integrand is a plane wave propagating in the $\mathbf{k}$ direction. A linearly polarized incident focused wave

$$\mathbf{E}_{inc}^{lin}(\mathbf{r}) = -\frac{iA}{\pi}\int_0^\alpha d\theta \int_0^{2\pi} d\phi \sin\theta\sqrt{\cos\theta}\exp(i\mathbf{k}\cdot\mathbf{r}) \begin{bmatrix} \cos\theta\cos^2\phi + \sin^2\phi \\ \cos\theta\cos\phi\sin\phi - \cos\phi\sin\phi \\ \sin\theta\cos\phi \end{bmatrix} \qquad (15)$$

can be rearranged to obtain

$$\mathbf{E}_{inc}^{lin}(\mathbf{r}) = -\frac{iA}{\pi}\int_0^\alpha d\theta \int_0^{2\pi} d\phi \sin\theta\sqrt{\cos\theta} \left[\cos\phi\exp(i\mathbf{k}\cdot\mathbf{r}) \begin{bmatrix} \cos\theta\cos\phi \\ \cos\theta\sin\phi \\ \sin\theta \end{bmatrix} \right.$$
$$\left. -\sin\phi\exp(i\mathbf{k}\cdot\mathbf{r}) \begin{bmatrix} -\sin\phi \\ \cos\phi \\ 0 \end{bmatrix}\right] \qquad (16)$$

The first and second terms in brackets in Eq. (16) can be recognized as TM_{inc} and TE_{inc} incident plane waves, respectively. We can write the total (incident + scattered) electric field due to scattering from spherical particles when the incident field is given by Eq. (15) as

$$\mathbf{E}_{tot}^{lin}(\mathbf{r}) = -\frac{iA}{\pi}\int_0^\alpha d\theta \int_0^{2\pi} d\phi \sin\theta\sqrt{\cos\theta} \left[\cos\phi\mathbf{E}_{tot}^{TM}(\mathbf{r}) - \sin\phi\mathbf{E}_{tot}^{TE}(\mathbf{r})\right] \qquad (17)$$

where $\mathbf{E}_{tot}^{TM}(\mathbf{r})$ and $\mathbf{E}_{tot}^{TE}(\mathbf{r})$ are defined in Eqs. (13) and (14), respectively.

A similar procedure can be applied when the incident beam is radially polarized, which is given by

$$\mathbf{E}_{inc}^{rad}(\mathbf{r}) = -\frac{iA}{\pi}\int_0^\alpha d\theta \int_0^{2\pi} d\phi \sin\theta\sqrt{\cos\theta}\exp(i\mathbf{k}\cdot\mathbf{r}) \begin{bmatrix} \cos\theta\cos\phi \\ \cos\theta\sin\phi \\ \sin\theta \end{bmatrix}. \qquad (18)$$

In this equation, the expression $\left(\cos\theta_{inc}\cos\phi_{inc}\hat{x} + \cos\theta_{inc}\sin\phi_{inc}\hat{y} + \sin\theta_{inc}\hat{z} \right)\exp(i\mathbf{k}\cdot\mathbf{r})$ is a representation of the TM polarized incident plane waves. Using the linearity of the integration operation, we can write the total field due to the radially polarized focused light as

$$\mathbf{E}_{tot}^{rad}(\mathbf{r}) = -\frac{iA}{\pi}\int_0^\alpha d\theta \int_0^{2\pi} d\phi \sin\theta\sqrt{\cos\theta}\,\mathbf{E}_{tot}^{TM}(\mathbf{r}) \tag{19}$$

where $\mathbf{E}_{tot}^{TM}(\mathbf{r})$ is defined in Eqs. (13).

In addition to the analytical solution, a three-dimensional finite element method (FEM) based solution is also obtained to calculate the response of spherical nanoparticles when they are illuminated with a focused beam of light. The FEM based solution will be validated using the analytical solution given in Section 3. The finite element method (FEM) is a well-known numerical algorithm for the solution of Maxwell's equations [22]. In this study, a frequency-domain based FEM is used for the solution of Maxwell's equations. Tetrahedral elements are used to discretize the computational domain, which allow modeling of arbitrarily shaped three-dimensional geometries. Over the tetrahedral elements, edge basis functions and second-order interpolation functions are used to expand the functions. Adaptive mesh refinement is employed to improve the coarse solution regions with high field intensities and large field gradients. To represent the focused incident beam, Eq. (6) along with Eqs. (4) and (5) are used with the FEM.
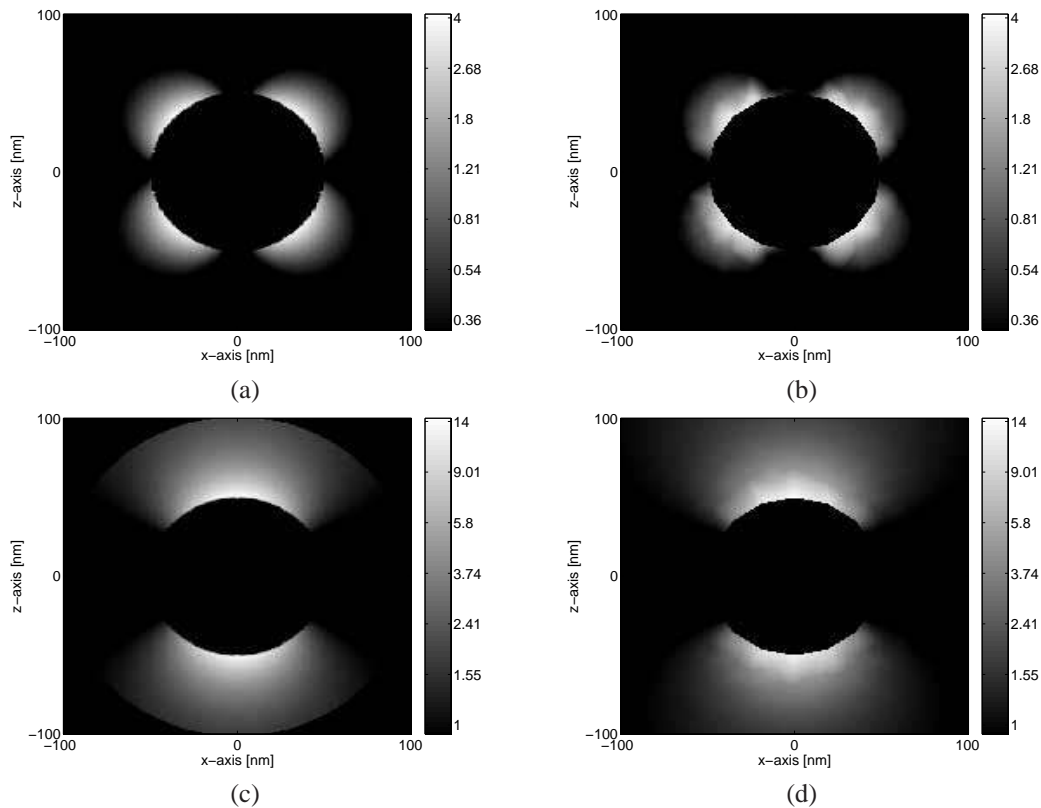
Fig. 4. Interaction of a radially polarized focused beam with a silver sphere with a 50 nm radius. The total electric field is plotted on the $\hat{x}$-$\hat{z}$ plane. (a) Solution using Mie series for $|E_x(x,y)|^2$, (b) FEM solution for $|E_x(x,y)|^2$, (c) Solution using Mie series for $|E_z(x,y)|^2$, (d) FEM solution for $|E_z(x,y)|^2$. $|E_y(x,y)|^2$ components for both solutions are negligible.

4. Results

In this section, we provide the results based on the methods outlined in Section 3. The analytical results are first compared with the FEM. Near-field electric field distributions of various dielectric and metallic spherical nanoparticles are investigated for highly focused linearly and radially polarized beams. The optical properties of materials in this section are taken from the literature [23].

To compare the results of the analytical solution with the FEM, three different spheres are considered: silver spheres with 50 and 250 nm radii, and a dielectric sphere with a 250 nm radius. The comparison of the results for the metallic spheres is crucial when investigating surface plasmons. Electromagnetic fields do not penetrate much into metallic spheres due to the small skin-depth of metal. Therefore, metallic sphere do not provide strong fields within the particles for comparison. Since electromagnetic fields penetrate better into a dielectric sphere, a comparison involving dielectric spheres provides an opportunity to validate the results within the sphere. Therefore, we will obtain the results for a dielectric sphere in addition to silver spheres. The wavelength for the calculations is 700 nm. The refractive index of the silver at this wavelength is taken from the literature [23] as $0.14 + i \times 4.523$. The wavelength is selected around the plasmonic resonances of larger nanoparticles. However, no particular attempt is made to optimize the response of the nanoparticles as a function of wavelength when they are

(a)

(b)

(c)

(d)
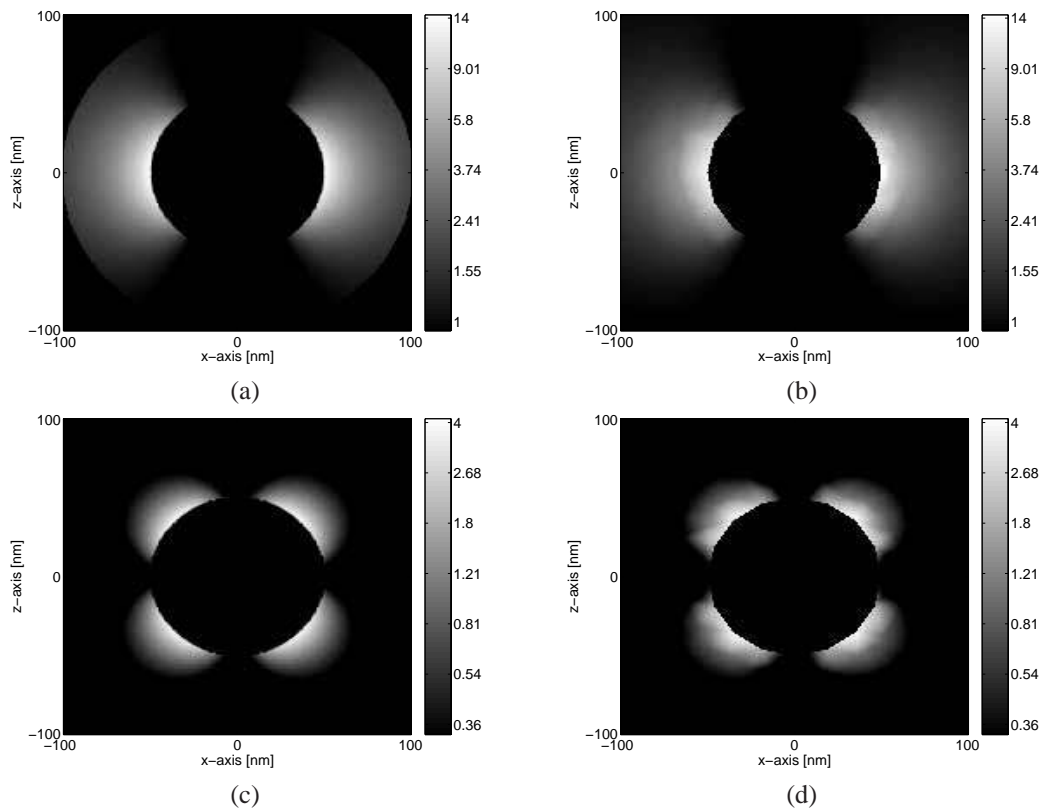
Fig. 5. Interaction of a linearly polarized focused beam with a silver sphere with a 50 nm radius. The total electric field is plotted on the $\hat{x}$-$\hat{z}$ plane. (a) Solution using Mie series for $|E_x(x,y)|^2$, (b) FEM solution for $|E_x(x,y)|^2$, (c) Solution using Mie series for $|E_z(x,y)|^2$, (d) FEM solution for $|E_z(x,y)|^2$. $|E_y(x,y)|^2$ components for both solutions are negligible.

illuminated with a focused beam of light.

In all simulations, the light propagates in the $+\hat{z}$ direction. In Figs. 4 and 5, the results of a silver sphere with a 50 nm radius are presented for radial and linear polarizations, respectively. The half beam angle of the optical lens is $60°$. In Figs. 4 and 5, $|E_x|^2$ and $|E_z|^2$ are plotted. The $|E_y|^2$ component was negligible for both linear and radial polarization. The Mie series solution agrees well with the FEM results. For the 50 nm sphere the results for radial polarization and linear polarization are very similar, except for a $90°$ rotation, which is consistent with the direction of the incident field at the focus, as shown in Figs. 1 and 2. In this case the sphere is too small to interact with field components in other directions.

The results for a silver sphere with a 250 nm radius is illustrated in Figs. 6 and 7 for radial and linear polarizations, respectively. The results again show agreement. The electromagnetic field distributions and the locations of maxima and minima are similar, especially for radially polarized wave. The amplitude of the electromagnetic field is in agreement both in the $\hat{x}$-direction and the $\hat{z}$-direction for radially polarized light. Although the amplitude of the electromagnetic wave in $\hat{z}$-direction is similar for linear polarization, there is some difference in the amplitude of the $\hat{x}$-component for linear polarization.

In the previous set of results for a 50 nm sphere in Figs. 4 and 5, we observed that the results of the radial and linear polarizations were similar, except for the $90°$ rotation. However, this
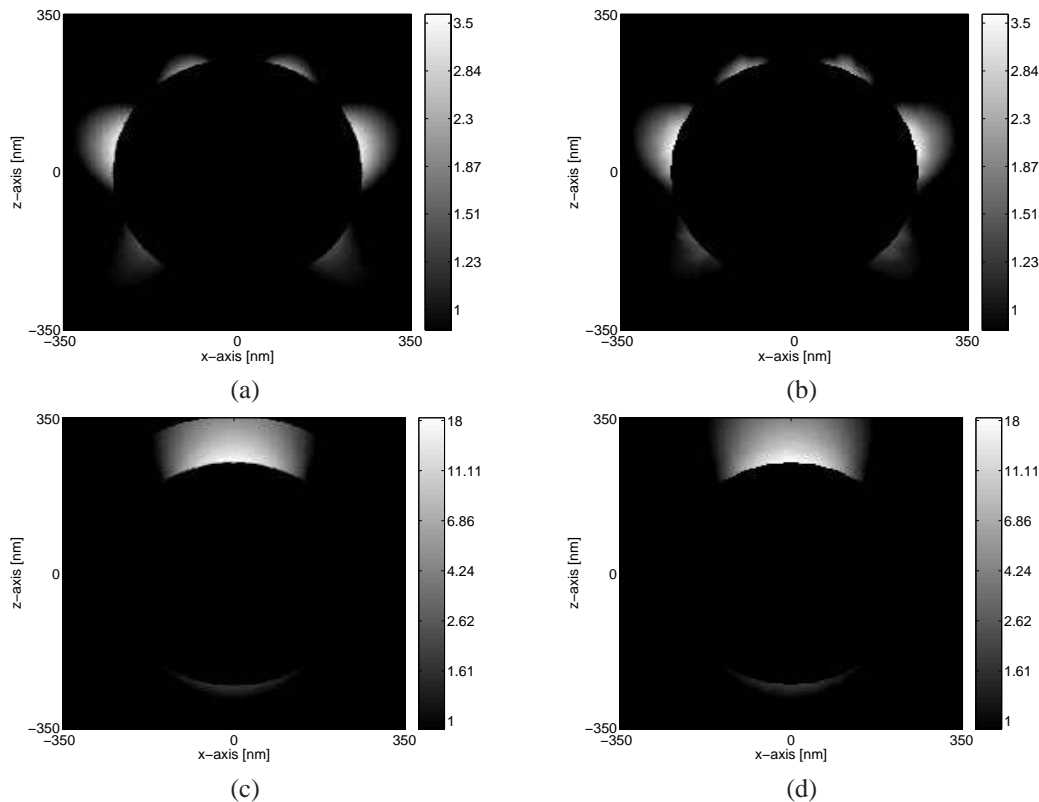
Fig. 6. Interaction of a radially polarized focused beam with a silver sphere with a 250 nm radius. The total electric field is plotted on the $\hat{x}$-$\hat{z}$ plane. (a) Solution using Mie series for $|E_x(x,y)|^2$, (b) FEM solution for $|E_x(x,y)|^2$, (c) Solution using Mie series for $|E_z(x,y)|^2$, (d) FEM solution for $|E_z(x,y)|^2$. $|E_y(x,y)|^2$ components for both solutions are negligible.
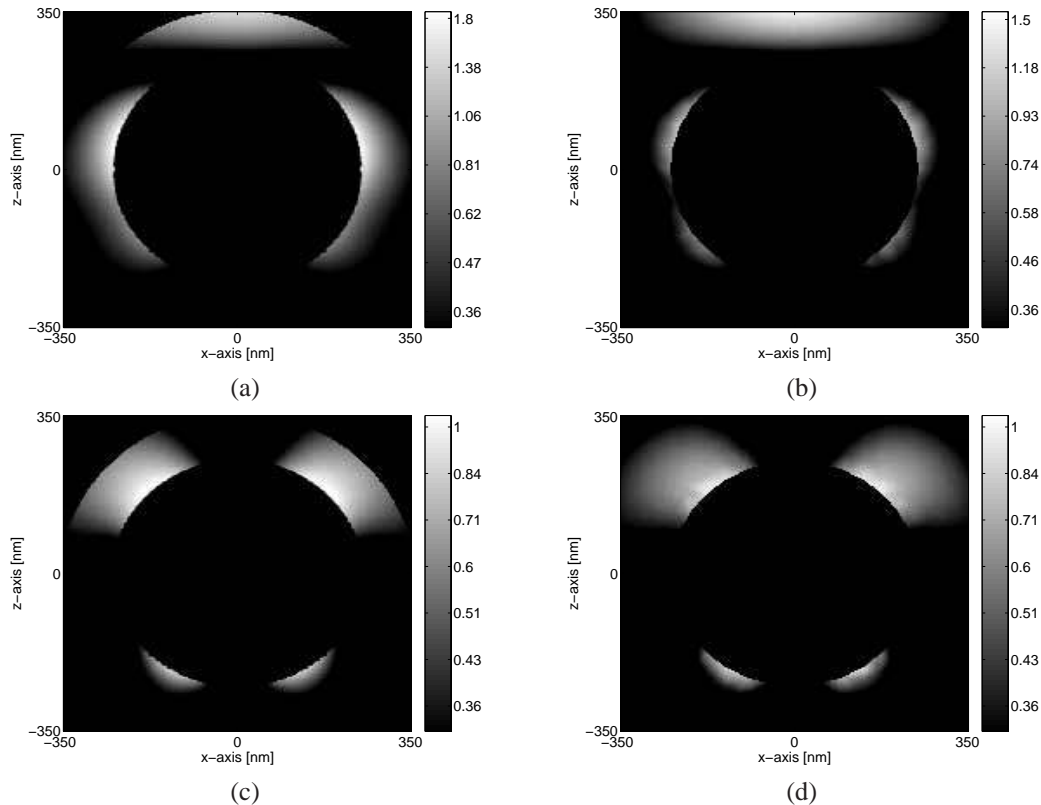
Fig. 7. Interaction of a linearly polarized focused beam with a silver sphere with a 250 nm radius. The total electric field is plotted on the $\hat{x}$-$\hat{z}$ plane. (a) Solution using Mie series for $|E_x(x,y)|^2$, (b) FEM solution for $|E_x(x,y)|^2$, (c) Solution using Mie series for $|E_z(x,y)|^2$, (d) FEM solution for $|E_z(x,y)|^2$. $|E_y(x,y)|^2$ components for both solutions are negligible.

similarity is not observed for the 250 nm sphere. For the 250 nm sphere case in Figs. 6 and 7, the results for the radial and linear polarizations are not rotated versions of each other. As the sphere gets larger, the nanoparticle at the focal area is more affected by the wide range of **k** vectors. The larger sphere feels the effect of various **k** vectors of the incident field outside the focal point, producing different electric field distributions in the scattered field. In the area around the focus, the main contribution for the linear and radial polarized light comes from the x-component and z-components, respectively. As shown in Figs. 1 and 2, the x-component for the linear polarization and the z-component of the radial polarization are similar. The other polarization components are small at the focus, therefore, a very small sphere does not feel the impact of these components. However, as the sphere becomes larger, it starts to feel the effect of the other polarization components. As shown in Figs. 1 and 2, the other polarization components have differences for linear and radial polarizations, which result in different response of the sphere for linear and radial polarizations. The amplitude of the $|E_z(x,z)|^2$ component is stronger than the $|E_x(x,z)|^2$ component.

In the analytical solution, the fields are represented using different spherical harmonics. The electromagnetic fields inside and outside the sphere in a Mie series solution is represented using different spherical harmonics. The continuity of the fields at the spherical boundary is enforced by the boundary conditions of the Maxwell's equations. Therefore, it is crucial to
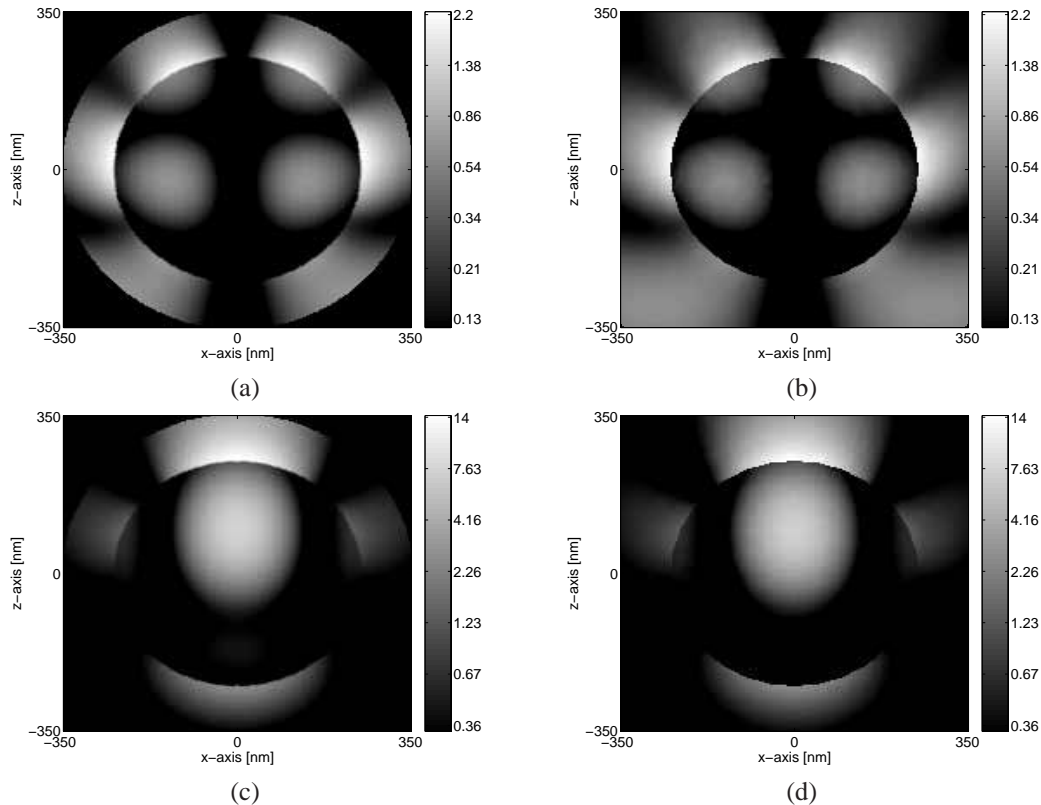
Fig. 8. Interaction of a radially polarized focused beam with a dielectric sphere with a 250 nm radius. Dielectic index of the sphere is 2. The total electric field is plotted on the $\hat{x}$-$\hat{z}$ plane. (a) Solution using Mie series for $|E_x\ (x,y)|^2$, (b) FEM solution for $|E_x\ (x,y)|^2$, (c) Solution using Mie series for $|E_z\ (x,y)|^2$, (d) FEM solution for $|E_z\ (x,y)|^2$. $|E_y\ (x,y)|^2$ components for both solutions are negligible.

check the validity of the results both inside and outside the sphere. Due to small skin-depth of metals, the electric field does not penetrate much into metallic spheres as shown in Figs. 4-7. It is, therefore, crucial to check the implementation inside the sphere for the analytical result by comparing it with the FEM. To test the electric field distributions inside the sphere, the interaction of a focused beam of light with a sphere with a radius of 250 nm and a dielectric index of 2 was calculated. Similar to the previous set of calculations, the half beam angle of the optical lens is 60°. Figures 8 and 9 illustrate the electric field distributions in the $\hat{x}$-$\hat{z}$ plane for radial and linear polarized incident light, respectively. The results are in agreement.

5. Conclusion

In this study, the interaction of spherical nanoparticles with highly focused incident beams was modeled using Richards-Wolf theory, which provides an accurate representation for a highly focused beam near the focus of an aplanatic lens. Both analytical and FEM-based models were developed to study this interaction. Formulations were given for both linearly and radially polarized focused beams. Analytical model and results in this study can be used by other scientists to validate more complicated 3-D modeling tools, such as FDTD and FEM involving linear and radial polarizations. In this study, the analytical model was also utilized to validate a 3-D FEM
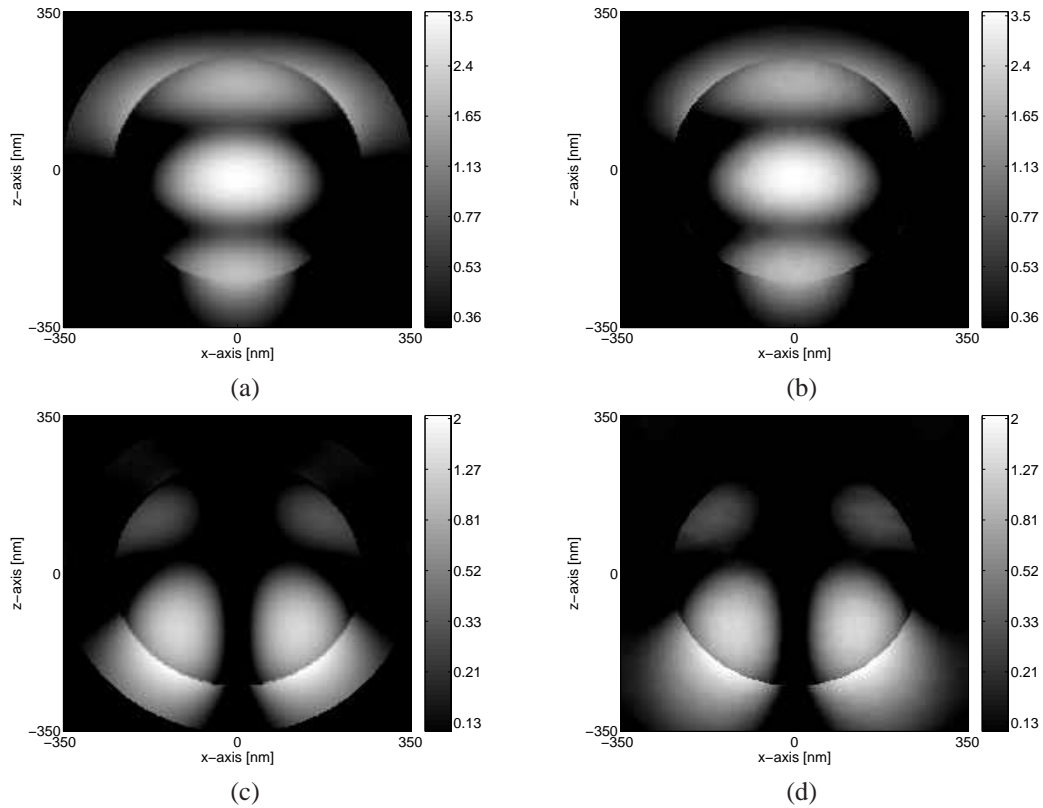
Fig. 9. Interaction of a linearly polarized focused beam with a dielectic sphere with a 250 nm radius. Dielectic index of the sphere is 2. The total electric field is plotted on the $\hat{x}$-$\hat{z}$ plane. (a) Solution using Mie series for $|E_x\,(x,y)|^2$, (b) FEM solution for $|E_x\,(x,y)|^2$, (c) Solution using Mie series for $|E_z\,(x,y)|^2$, (d) FEM solution for $|E_z\,(x,y)|^2$. $|E_y\,(x,y)|^2$ components for both solutions are negligible.

solution. There has been increasing interest in radially polarized focused beams to excite surface plasmons on nanoparticles. The tools developed in this study are crucial to validate and analyze the interaction of particles with linear and radial polarizations.